TRANSPORT PROBLEMS 2023 Volume 18 Issue 2
PROBLEMY TRANSPORTU DOI:10.20858/tp.2023.18.2.09

Keywords: civil engineering; transport; crane bumper; welding; FEM, hybrid calculations

Tomasz HANISZEWSKI[1]*, Tomasz WĘGRZYN[2], Bożena SZCZUCKA-LASOTA[3]

IMPACT ANALYSIS OF MICRO-JET COOLING FOR STRESS CONCENTRATION IN A CRANE BUMPER DURING A COLLISION

Summary. In the structure of crane bumpers, there is a need to join various types of steel. Usually, low-alloy steel structures are used for this purpose, which can be represented by S355J2 steel. The tensile strength of S355J2 low-alloy steel is slightly below 600 MPa, and the tensile strength of S355J2 steel is at the high level of 200 J at ambient temperature. The impact strength of this steel in negative temperatures is also good at over 47 J at -60 °C, so it meets the 6th class of impact toughness. Welding structures, after classic gas metal arc welding (GMAW) processes, meet only the second impact toughness class. An improved GMAW process was used by micro-jet cooling application to raise the mechanical properties of the joints. The microstructure and main properties of the joints were carefully analyzed. The influence of using the new suggested welding process on the various properties of the welds is presented (UTS – ultimate tensile strength, YS – yield strength, Poisson ratio, elongation, Young's modulus). Then, the effects of tests for use in crane bumper construction were checked by using a hybrid finite element method (FEM) analysis.

1. INTRODUCTION

In civil engineering and transport, steel welding combined with cooling by micro-jet injector might displace the existing gas metal arc welding (GMAW) process because of the large difference in impact toughness [1]. The first aim of the paper is to present the research results of the possibility of GMAW with direct cooling (by micro-jet stream) for a crane bumper thin-walled structure. The possibility of correct GMAW welding and repeatable joints with much better mechanical properties were correctly tested. Welded joints with better properties may affect new design constructions of crane bumpers with increased lifting capacity and, therefore, working range. Overhead cranes are often found in various industrial applications. There are situations where the system that controls the speed of the trolley or girder does not work properly. Due to these irregularities, there is a risk of the trolley colliding with the buffer with significant force. Secondly, this article aims to present hybrid simulation models that allow the simulation of the impact of the crane trolley system on the bumper and to determine the forces acting on the supporting structure. Then, the determined forces are adapted to the numerical model of the structure using Finite Element Method (FEM) software. The influence of impact on welds was taken into account using changes in the microstructure of the weld. The influence of weld modeling on the stress state at impact was also investigated.

[1] Silesian University of Technology, Faculty of Transport and Aviation Engineering, Krasińskiego 8, 40-019 Katowice, Poland; e-mail: tomasz.haniszewski@polsl.pl; orcid.org/0000-0002-4241-6974
[2] Silesian University of Technology, Faculty of Transport and Aviation Engineering, Krasińskiego 8, 40-019 Katowice, Poland; e-mail: tomasz.wegrzyn@polsl.pl; orcid.org/0000-0003-2296-1032
[3] Silesian University of Technology, Faculty of Transport and Aviation Engineering, Krasińskiego 8, 40-019 Katowice, Poland; e-mail: e-mail: bozena.szczucka-lasota@polsl.pl; orcid.org/0000-0003-3312-186
* Corresponding author. E-mail: tomasz.haniszewski@polsl.pl

Without proper cooling, large temporal temperature gradients and temperature levels can occur that degrade a welding structure and lead to cracks in the microstructure. The resulting structures limit the product performance and constrain life. Conventional cooling methods, such as natural cooling after the welding process, sometimes take too long to obtain the correct structure. The cooling methods described in the literature (Table 1) have limited cooling capacities or sometimes unacceptably high power consumption. They are also not suitable for use in welding processes. Therefore, other solutions, such as advanced water or inert gas cooling techniques, are in demand.

Table 1

Micro-jet cooling systems solutions

Work in which the solution is presented	**Can it be used in the welding process?**
Raschid Bezama, Govindarajan Natarajan, United States Patent nr US20070227173A1, High power microjet cooler, 26.05.2009	NO
Koninklijke Philips NV, Cooling assembly with micro jet, Patent nr JP4298746B2, 22.07.2009	NO
Douglas J. Woodruff Michigan, Micro-jet cooling of cutting tools, Patent US8439609B2, Technological University, 2009	NO
Sung, M.K. & Mudawar, I. (2008). Single-phase hybrid micro-channel/micro-jet impingement cooling. International Journal of Heat and Mass Transfer, 51(17–18). https://doi.org/10.1016/j.ijheatmasstransfer.2008.02.023	NO
Chen, W., Luo, X. B., Cheng, T., Huang, S. Y., & Liu, S. (2007). Experimental investigation on micro jet cooling system for high power LED. Bandaoti Guangdian/Semiconductor Optoelectronics, 28(4).	NO
Kim, S. H., Shin, H. C., & Kim, S. M. (2019). Numerical study on cooling performance of hybrid micro-channel/micro-jet-impingement heat sink. Journal of Mechanical Science and Technology, 33(7). https://doi.org/10.1007/s12206-019-0649-7	NO
Barrau, J., Omri, M., Chemisana, D., Rosell, J., Ibañez, M., & Tadrist, L. (2012). Numerical study of a hybrid jet impingement/micro-channel cooling scheme. Applied Thermal Engineering, 33–34(1) https://doi.org/10.1016/j.applthermaleng.2011.10.001	NO
Szczucka-Lasota, B. Materials and equipment in HM ultrasonic thermal spraying method for high corrosion resistance coatings applied in power energy, Gliwice, Poland, 2017	METHOD – YES in MAG, MIG, TIG SIDE DISH –NO
Szymczak, T. at al. (2021). Behavior of weld to 960mc high strength steel from joining process at micro-jet cooling with critical parameters under static and fatigue loading. Materials, 14(11). https://doi.org/10.3390/ma14112707	YES in MAG, MIG, TIG

Micro-jet cooling is a new solution introduced to the welding process. Micro-jet cooling is a new technology that could be regarded as a new way to change an obtained welded structure and improve its mechanical properties [2-4]. Cooling at the right speed with a narrow gas stream allows the structure to be controlled. This means that providing appropriate cooling conditions makes it possible to obtain welds with a smaller or larger gradation of grain in the structure and, thus, to change the mechanical properties of the joint.

2. PURPOSE AND OBJECTIVE OF THE RESEARCH

The object of consideration in this article is an unusual construction of an overhead crane with a total lifting capacity of 5 t. Table 2 [5] presents its general characteristics, and Fig. 1 shows its construction.

As shown in Fig. 1, there is a trolley pendulum system connected to a series system of buffers based on rubber material. The considered model includes bumpers, its steel structure, and a trolley with a load on a flexible rope. The buffer consists of two parts: a steel structure and a rubber buffer. For further calculations, the impact velocity against the buffer was assumed to be 0.6 m/s. The main purpose of the article is to examine the behavior of the cart pendulum system at the moment of impact of the bumper at the end of the girder with a selected speed and its impact on the stress concentration on the welded parts of the bumper using different material parameters depending on the cooling in the welding process. A rubber bumper type was selected for testing.

Table 2

Technical data of the considered construction

Description		Symbol	Dimension	Value
Lifting capacity		Q	t	5
Span		L	m	20
Lifting height		H	m	16
Operating speed	Lifting	v_h	m/s	0.208
	Winch driving	v_j	m/s	0.6
Maximum impact force at the bumper at $0.5v_j$		Z_u	N	$30 \cdot 10^3$
Braking distance at $0.5v_j$		S_h	m	0.52

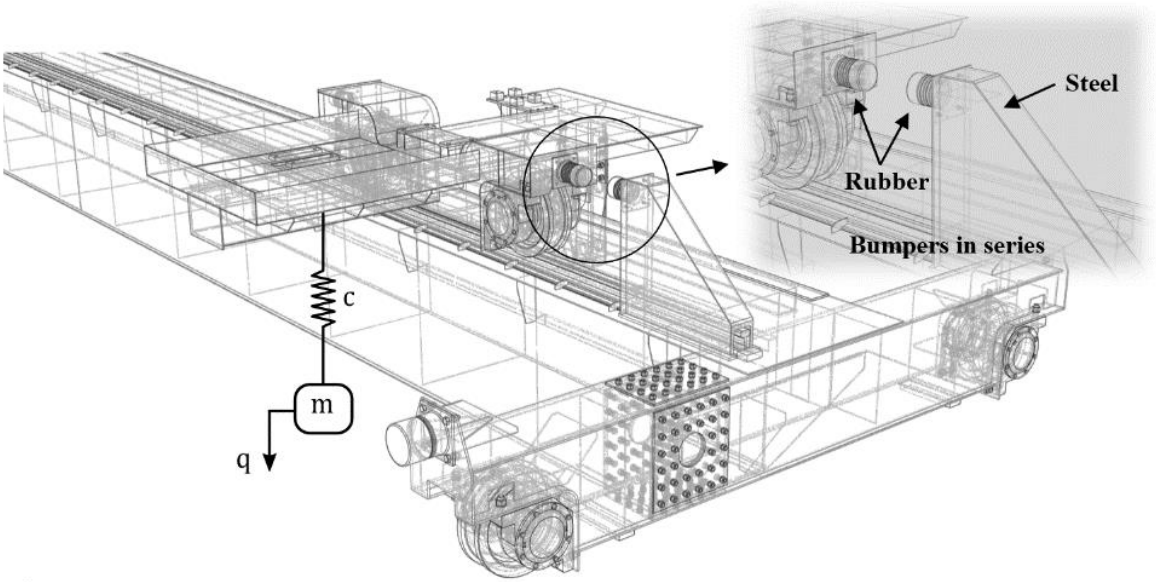

Fig. 1. Considered construction of a crane

Using the 3D model presented in Fig. 1, the (FE) Finite Element numerical model was built in the Autodesk Inventor software [6], which was then used to analyze the stress concentration in the given welded joints with micro-jet cooling.

3. RESEARCH MATERIALS AND WELDING PARAMETERS

Low-alloy steels are treated as well-weldable materials. From the available group of materials, S355J2 was chosen. The chemical composition of the tested material (i.e., S355J2 steel) is presented in Tab. 3. It is precisely shown that carbon content is 0.2%, which increases the strength, while the Ni amount is at the level of 0.35%, which improves the impact strength. The most important mechanical properties are presented in Table 4. Fig. 2 presents a steel construction of a buffer with characteristic

dimensions and welding parameters. The base steel plate of the construction is welded with a 4-mm-wide fillet weld, and the base is welded with a 3-mm-wide fillet weld *in* the construction of the buffer.

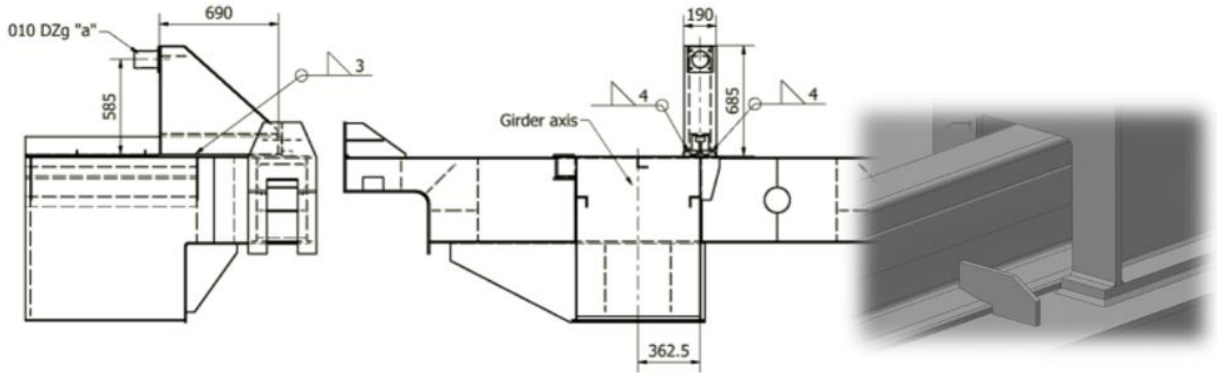

Fig. 2. The considered bumper on a crane construction

Table 3

Composition of S355J2 steel

Steel	C, %	Mn, %	Si, %	P, %	S, %	Al, %	Ni, %	Cu, %
S355J2	0.2	1.52	0.4	0.03	0.03	0.02	0.35	0.02

Table 4

Mechanical properties of S355J2 steel

Mechanical property	Value
Poisson's ratio	0.28
Impact toughness (at -20 °C), [J]	50
Tensile strength [MPa]	590
Yield strength [MPa]	380
Elongation [%]	14
Young's modulus [GPa]	205
Hardness [HB]	220

Table 4 shows that Young's modulus is 205 GPa. It is worth recalling that after welding, Young's modulus value increases, which is important from the point of view of crane welded constructions. After classic welding processes, Young's modulus unfavorably rises to as much as 220-235 GPa depending on the kind of welding process used. This is related to the structure of the weld, which should be characterized especially by the size of ferrite grains. In the classic welded joint made of unalloyed steel, a high Grain Boundary Ferrite (GBF) content is observed, which is unfavorable; a low content of fine-grained ferrite is much more beneficial. S355J2 steel should be welded with limited, linear energy (max. 5 kJ/cm) to achieve a beneficial structure with as little GBF content as possible and with a respectable lifted amount of fine ferrite. Low-alloy steels might be welded by applying processes that guarantee low hydrogen, low nitrogen, and low oxygen content in a weld metal deposit (WMD) [7-9].

4. SAMPLE PREPARATION

S355J2 steel joints were made using typical electrode wire SG3 (DIN 8559; EN ISO 14341-A) with a typical low alloy composition (C=0.081%; Si=0.83; Mn=1.71%). The mechanical properties of the WMD of the tested wire are shown in Table 5.

Table 5

Main properties of the WMD

Mechanical property	Value
Strength, MPa	600
Yield point, MPa	460
Impact toughness (at -40 C), J	50
Elongation, %	17

The composition of both the steel S355J2 and electrode wire SG3 could be treated as similar. Both materials have a similar chemical composition, which may have a corresponding effect on the comparable plastic properties of the joint. The 6-mm thickness was used for welding in the butt weld position. Before welding, the sheets had dimensions of 600×200×6 mm. In the tests, butt joints with a bevel on the V were made.

The steel welding parameters are presented below:

- Welding wire diameter: 1 mm
- Welding current: 115 A
- Arc voltage: 19 V

CORGON-18 (82% Ar-18% CO_2) was chosen as a shielding gas mixture with a flow rate of 15 L/min. The welding speed was 400 mm/min. A micro-jet cooling injector was installed during the GMAW process with the following parameters:

- Argon or helium as a cooling medium;
- Jet diameter: 70 μm;
- Micro-jet gas (Ar or He) pressure was varied twice: 0.6 and 0.7 MPa.

Research methods: Non-destructive tests (NDTs) and some further destructive tests of welds were realized. NDTs were presented by visual tests (VTs) according to PN-EN-ISO 17637 requirements. Next, the magnetic-particle tests (MTs) were done based on EN-ISO-17638 (using REM-230 magnetic flaw detector). The destructive tests were mainly based on tensile strength measurements and microstructure analysis according to the PN-EN-ISO-15614-1 standard. Tensile tests were done on a ZWICK 100-N5-A machine.

Research results and discussion: Both the VTs and MTs confirmed that all welds were made correctly. In NDTs, no non-conformities or welding defects were found. The next part of the investigation was tensile strength tests, which were prepared according to PN-EN-ISO-4136:2013;05.

The tensile test results (average of three stretches) are given in Table 6.

Table 6

Mechanical properties of welds

Micro-jet gas	Micro-jet pressure, MPa	Re, MPa	Rm, MPa	A_5	E, GPa	*v*
None	–	351	554	12.1	229	0.31
Argon (Ar)	0.6	359	567	13.1	214	0.34
Helium (He)	0.6	362	572	13.2	213	0.35
Argon (Ar)	0.7	368	581	14.0	211	0.37
Helium (He)	0.7	373	583	14.1	210	0.38
Argon (Ar)	0.8	348	559	13.3	215	0.33
Helium (He)	0.8	347	557	13.2	216	0.32

The table data shows that the use of a micro-jet injector can be very beneficial in the GMAG process. Tensile strength was lifted from 554 MPa up to 583 MPa (when He was used). The important benefit is the increase of elongation from 12.1 to max. 14.1%. It was observed that He is a preferred micro-jet gas

over Ar (due to its better thermal conductivity). It has been shown that micro-jet cooling also affects Poisson's ratio and Young's modulus values. The mechanical properties correspond to the structures. Micro-jet welding allows the metallographic structure to be controlled. The etching agent Nital was used to prepare microscope observations. Nital is a solution of nitric acid in ethyl alcohol commonly used for the chemical etching of ferrous metals. The digestion of the microsection took eight seconds. The effect of using the micro-jet illustration in the welding of the structure is shown in Figs. 3 and 4.

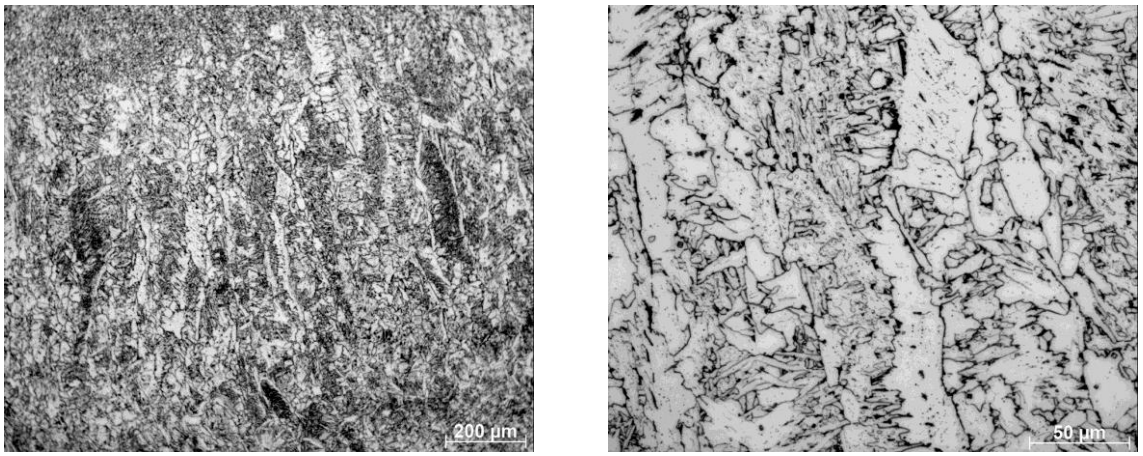

Fig. 3. Grain boundary ferrite in a weld without micro-jet cooling (etched, Nital)

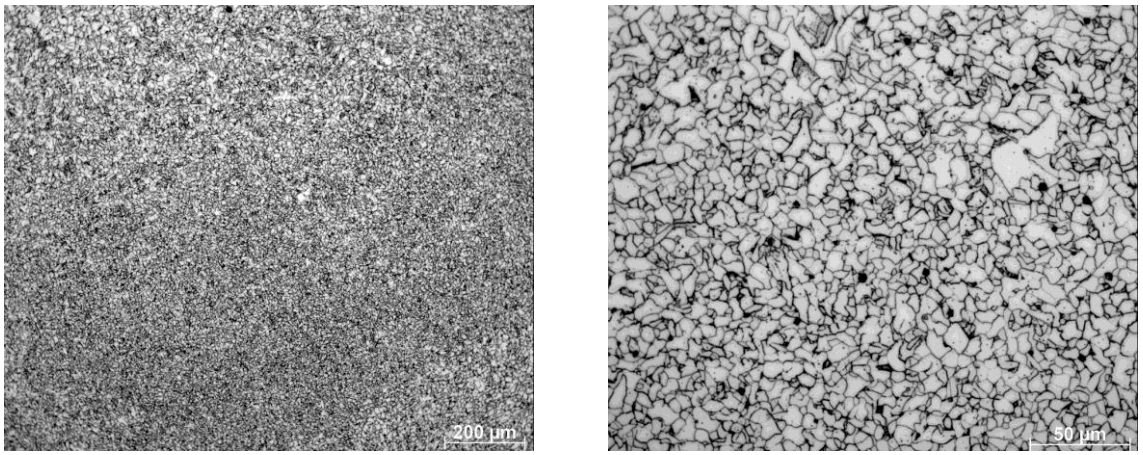

Fig. 4. Fine ferrite in weld after welding with helium micro-jet cooling (etched, Nital)

The analysis of the drawings shows a significant fragmentation of the ferrite grain, which translates into a change in the mechanical properties of the joint. As the average grain size decreases, tensile strength and yield strength increase. This pattern is clearly shown in Figs. 3 and 4.

5. PHENOMENOLOGICAL MODEL OF THE RESEARCH OBJECT

The subject of this part of the article is the trolley-pendulum model, the mathematical model of which was presented and used to simulate the movement of the crane trolley. Referring to the topic introduced in the Introduction to the article, Fig. 5 shows a dynamic model of a horizontally moving mass equipped with a pendulum with a flexible steel rope in case of the absence of damping [4, 10-12]. The data describing the physical model are set in Table 7 [5].

Fig. 5 presents a cart-pendulum dynamic model that is well-known in the literature [3, 13-17]. Mass m represents a load acting on a wire rope, and it relates to elastic wire rope represented by stiffness c_l. Mass m_w is the mass of the cart itself. The damping coefficient described by b is also added into the considered model, and it is used for adopting friction influence between wire rope and rope drum.

Moreover, b_1 and c_1, as well as c_2 and b_2, are parameters adopted for the simulation of the rubber buffer. Next, an inverted physical pendulum is added to the model. This type of pendulum represents a construction of a buffer holder, where h_{zd} is its height and m_{zd} is its mass. Parameters b_{zd} and c_{zd} are the rotational damping and stiffness of a buffer holder construction. The model that represents the simulation of a collision of the cart-pendulum system with a buffer is shown in Fig. 5. By adding to a model gap δ, which is presented in Equation (3), we were able to simulate the collision.

Table 7

Physical parameters describing the dynamic system

L.p.	Mark	Value	L.p.	Mark	Value
1	m	$1800\ kg$	10	δ	$1\ m$
2	m_w	$2020\ kg$	11	h_{zd}	$0.585\ m$
3	m_{zd}	$47\ kg$	12	c_{zd}	$40.5 \cdot 10^6\ Nm/rad$
4	v_j	$0.6\ m/s$	13	b_{zd}	$8.3 \cdot 10^4\ Nms/rad$
5	d_{wire_rope}	$12 \cdot 10^{-3}\ m$	14	c_l	$1.04 \cdot 10^8\ N/m$
6	g	$9.81\ m/s^2$	15	c_z	$8.5 \cdot 10^5\ N/m$
7	μ	0.05	16	J_{zd}	$5.36\ kgm^2$
8	l	$0.5\ m$	17	b_z	$1.7 \cdot 10^3\ Ns/m$
9	b	$1 \cdot 10^3\ Ns/m$			

On the basis of the dynamic model presented in Fig. 5, equations of motion were formulated. In the considered system, the velocity of mass *m* added to the end of the wire rope is represented by Formula (1):

$$V_c^2 = 2\dot{\Theta}\cos\Theta\,(l+y)\dot{x}_q + \dot{\Theta}^2(l+y)^2 + 2\dot{y}\dot{x}_q\sin\theta + \dot{x}_q{}^2 + \dot{y}^2 \tag{1}$$

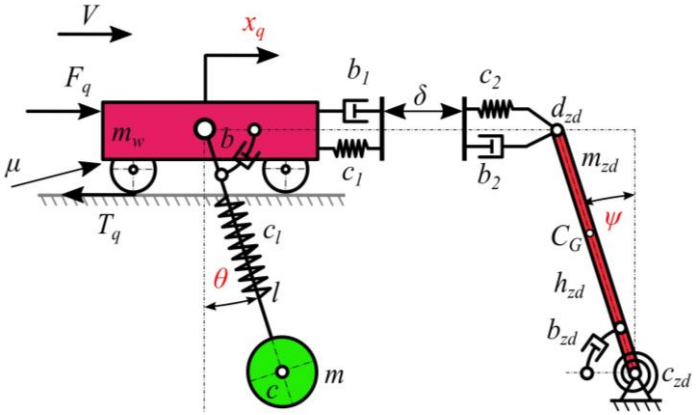

Fig. 5. The physical model of a cart-pendulum system with a classical bumper [5]

After applying the second kind of Lagrange equations [2] and taking into account the assumed mathematical formula defining excitations, the system of four non-linear differential equations was obtained as shown below:

$$\begin{gathered}
(y+l)^2\ddot{\Theta} + 2(y+l)\dot{y}\dot{\Theta} + bm^{-1}\dot{\Theta} + gl\sin\Theta + (y+l)\ddot{x}_q\cos\Theta = F_q \\
\ddot{y} + c_l m^{-1} y - (y+l)\dot{\Theta}^2 + \ddot{x}_q\sin(\Theta) = 0 \\
(m_w+m)\ddot{x}_q + m(y+l)\cos\Theta\,\ddot{\Theta} - m(y+l)\sin\Theta\,\dot{\Theta}^2 + 2m\dot{y}\,\dot{\Theta}\cos\Theta + m\ddot{y}\sin\Theta \\
= -\left(\mu g(m_w+m)sign\dot{x}_q\right) + F_z \\
h_{zd}{}^2 m_{zd} 3^{-1}\ddot{\psi} + b_{zd1}\dot{\psi} + c_{zd1}\psi - g h_{zd} m_{zd}\sin\psi = -h_{zd}F_z
\end{gathered} \tag{2}$$

where:

$$F_z = \begin{cases} 0, & |\xi| \le \delta \\ c_z\left(\xi - \delta sgn(\xi)\right) + b_z\left(\frac{d}{dt}\left(\xi - \delta sgn(\xi)\right)\right), & |\xi| > \delta \end{cases} \tag{3}$$

$$\xi = h_{zd}\psi - x_q, c_z = \frac{c_1 c_2}{c_1 + c_2}, b_z = \frac{b_1 b_2}{b_1 + b_2}.$$

6. RESULTS OF HYBRID SIMULATION

The research plan assumes the creation of a series of simulations on the selected model to obtain forces acting on buffer construction. Two speeds were considered at the point of impact. The speeds considered are 0.3 and 0.6 m/s, and the length of the rope is 0.5 m with a 1-m gap between the cart and buffer. The used force F_q as an excitation was added to induce speed as mentioned earlier. In all cases, the force F_q was included as a value rising from zero to a specific value for assumed velocity within one second.

As shown in Fig. 7, there are spikes of force acting on a bumper. The maximum value of force is about 25 kN for a 0.5-m wire rope length. At lower speeds, the maximum force value is about 12 kN. We can also observe a rebound effect, which is connected with a constant acting force. This special case is related to the actual situation of braking system failure. Fig. 8 displays a large deceleration associated with the collision. As shown, the value is greater than 1 g for a velocity of 0.6 m/s and approximately 0.5 g for lower speeds.

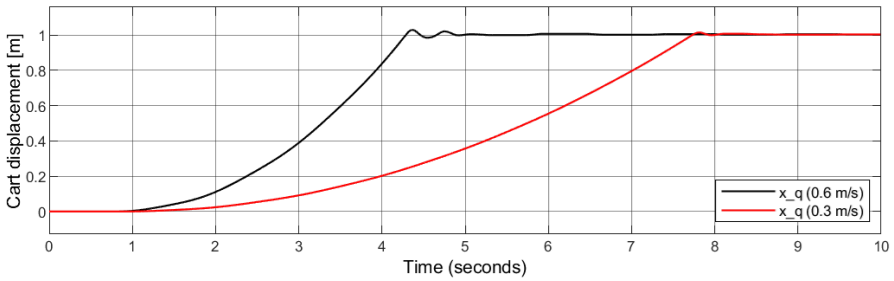

Fig. 6. Time waveforms of the trolley displacement along the x-axis for the rope length of 0.5 m

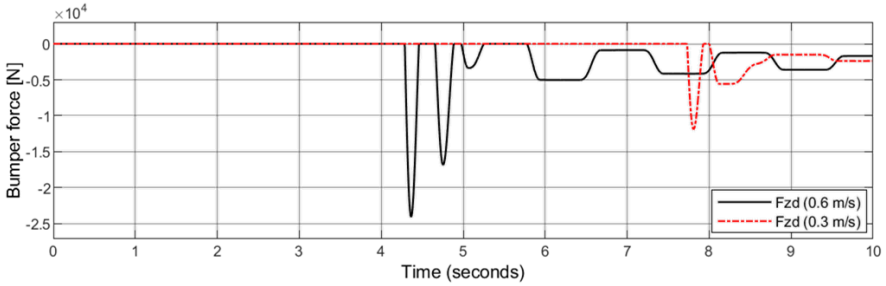

Fig. 7. Time waveforms of the bumper force along the x-axis for the rope length of 0.5 m

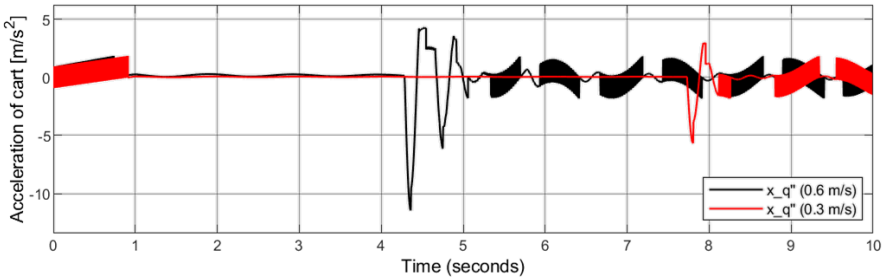

Fig. 8. Time waveforms of the cart acceleration along the x-axis for the rope length of 0.5 m

Hybrid calculations were carried out using the FE method. A geometric model of the tested structure was used based on the construction documentation. Fig. 9 shows part of the structure with a buffer.

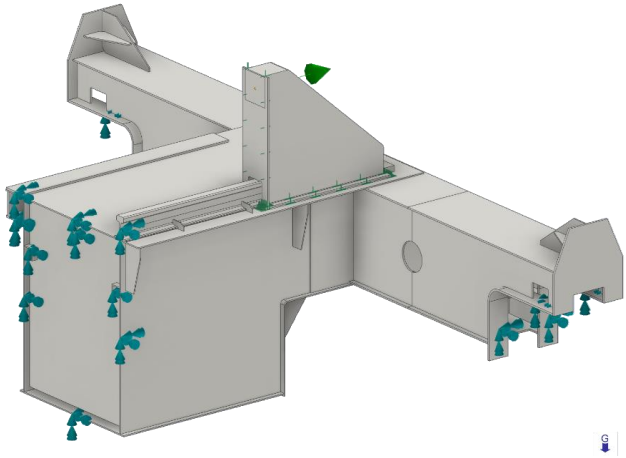

Fig. 9. FEM model of considered object (couplings and constraints)

For the analysis, two types of materials were selected for testing. The first is rubber, and the second is S355J2 steel, with different parameters depending on whether a weld or a normal material was used. Boundary conditions at the location are presented in Fig. 9. In the discussed nodes, all degrees of freedom were received in both supports, in the place where the wheelsets were assembled, degrees of freedom along the axis along the girder and rotations in the axis of the steering wheel was released.

Material data of selected materials are shown in Tables 6 and 8. Based on the geometric model presented in Fig. 9, the FE numerical model was created. The model was loaded with a static force of 25 kN obtained in the numerical simulation presented in the phenomenological model shown in Fig. 5. The simulation results are shown below.

Table 8

Material data [5, 6]

Rubber, natural		
Density	ρ	$930\ g/m^3$
Poisson's coefficient	ν	0.5
Young's modulus	E	$3 \cdot 10^6 Pa$
S355J2		
Density	ρ	$7850\ g/m^3$
Poisson's coefficient	ν	0.28
Young's modulus	E	$2.05 \cdot 10^{11}\ Pa$

As shown in Fig. 10, there are specific points of concentration of stresses. For a better view, there are presented stress maps with isolines, which also include an impact force and boundary conditions. As the presented model does not take into account material changes in the welding process, the impact of changes in weld parameters on the simplest model is presented below, depending on the welding process used and the numerical model used.

As presented earlier in Table 5, Young's modulus and Poisson's ratio change depending on the method of cooling the weld. For analysis, three cases were compared, the weld entirely consisting of native material (i.e., S355J2), a weld material with properties for an uncooled system and for helium-cooled material. Due to the highly problematic modeling of welded joints, three methods of weld modeling are presented.

The first includes the weld model as a fillet connected to the material of the structure using bonded contact, and the joint between two perpendicular welded parts is considered as frictionless contact (i.e., we assume a weld without penetration) (Fig. 12a). Subsequently, a change was assumed in the form of

remelting on the contact surface of the connected structural elements (Fig. 12b). The last change concerns the consideration of full penetration (Fig 12c). Based on the discussed modeling methods and material data, the results below are presented for 18 numerical simulations (Table 9), including the dynamic load of the sample as force described by the function shown in Fig. 11. For dynamic, implicit simulations, the materials considered were determined damping parameters as Rayleigh damping for coefficients $\alpha = 0.001$ and $\beta = 0.0001$.

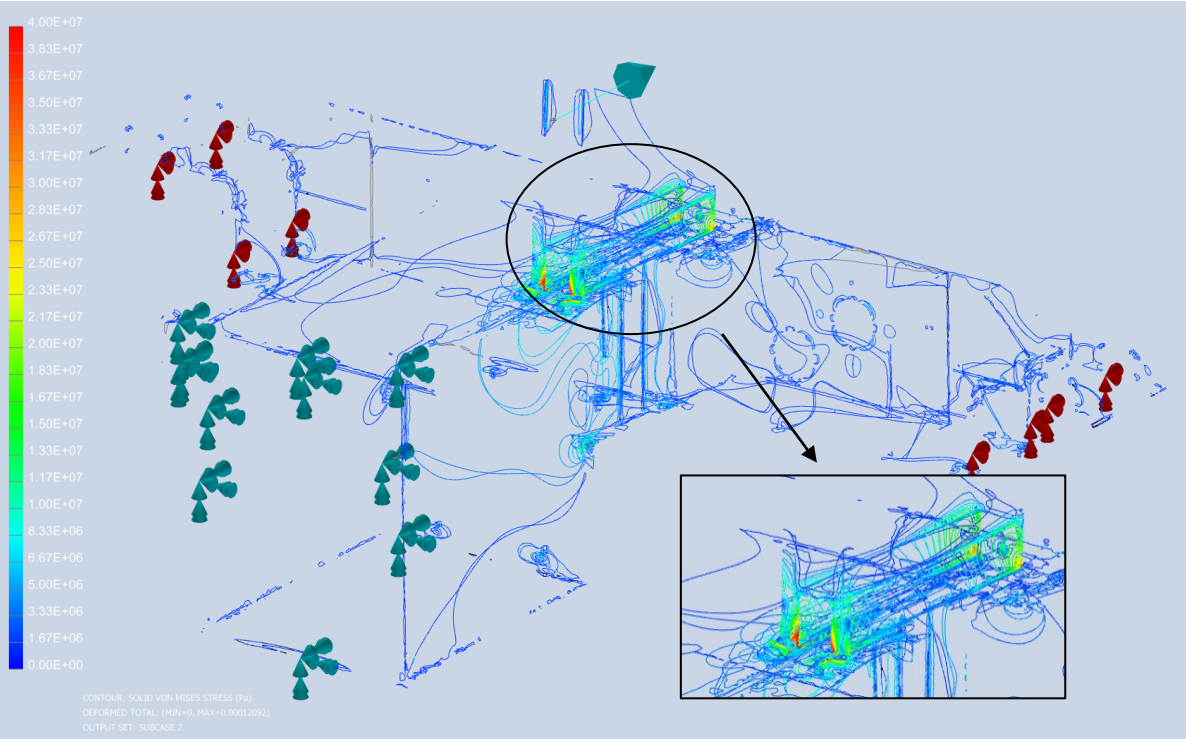

Fig. 10. Stress reductions according to the Huber-Mises-Hencky theory, isolines of stresses in a considered construction

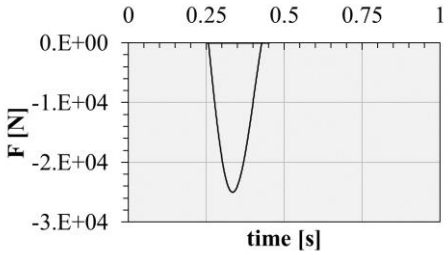

Fig. 11. Force shape function representing the dynamic load shape of the test specimen on impact

The results will be given as differences from the base solution to show the impact of modeling changes in weld material data, thereby enhancing the illustrative nature of the calculations. The base solution includes a homogeneous native weld material.

The test results are summarized in Table 9, where the reading is divided into three categories: maximum values including imperfections, maximum values excluding imperfections, and maximum values outside the welding area.

As can be seen, based on the tests carried out (Figs. 13, 14, 15), the largest differences in the results were obtained at the edges of imperfections, particularly for the model in which the non-cooled material was taken into account and the weld was modeled as penetration weld. The difference in relation to the base model is as much as 15.82%; for the model with no penetration weld, this value is 14.69%. In the case of uncooled weld material, for the model with a full penetration weld, a stress decrease of about 1% was noted.

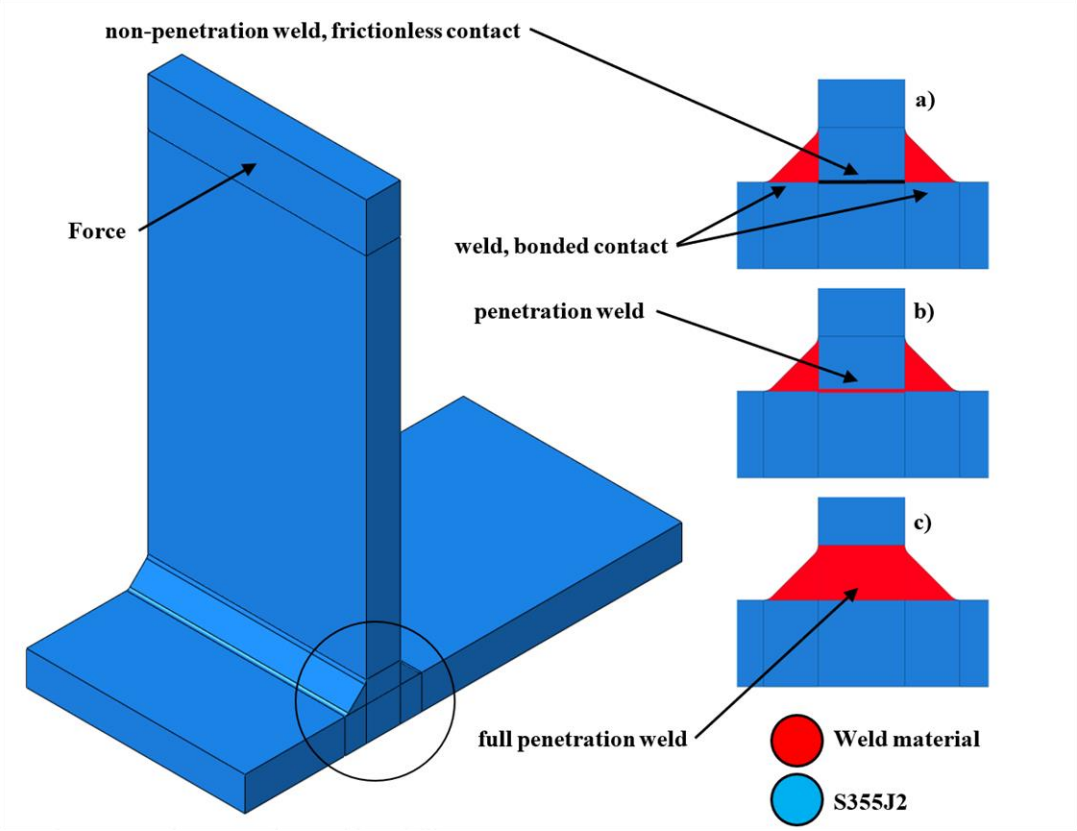

Fig. 12. The test sample, approach to weld modeling

Table 9

Results of simulation tests

	No penetration weld	Penetration weld	Full penetration weld
	Imperfections		
Weld uniform material	0.00%	0.00%	0.00%
Weld uncooled material	14.69%	15.82%	-1.16%
Welded helium-cooled material	11.86%	11.91%	-7.88%
	No imperfections		
Weld uniform material	0.00%	0.00%	0.00%
Weld uncooled material	-0.18%	2.68%	-1.42%
Welded helium-cooled material	-1.90%	3.23%	-9.65%
	Outside the weld		
Weld uniform material	0.00%	0.00%	0.00%
Weld uncooled material	0.19%	0.18%	0.39%
Welded helium-cooled material	0.33%	0.32%	1.19%

Similar differences were obtained for the helium-cooled material, whereas a stress reduction on imperfections as high as 7.88% was obtained for the full penetration weld. If imperfections are bypassed, only the helium-cooled material achieved a 9.65% stress reduction. Taking into account the rest of the structure (bypassing the weld area), regardless of the modeling method or material properties of the welds, the stress values remain the same.

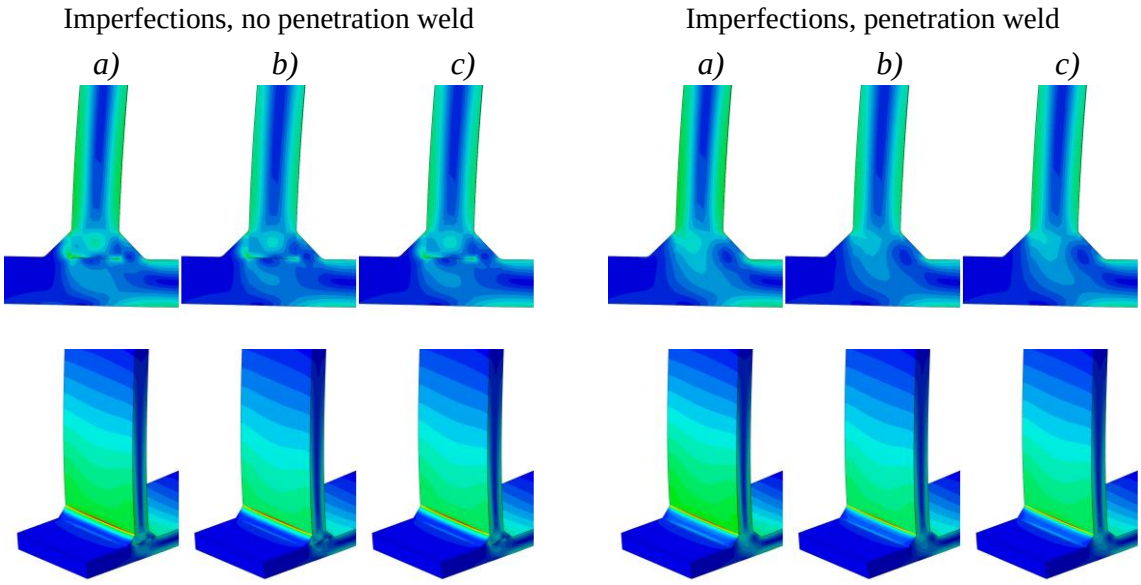

Fig. 13. Results of simulation tests (stresses reduced according to the Huber-Mises-Hencky theory): a) Weld uniform material, b) weld uncooled material, and c) welded helium-cooled material

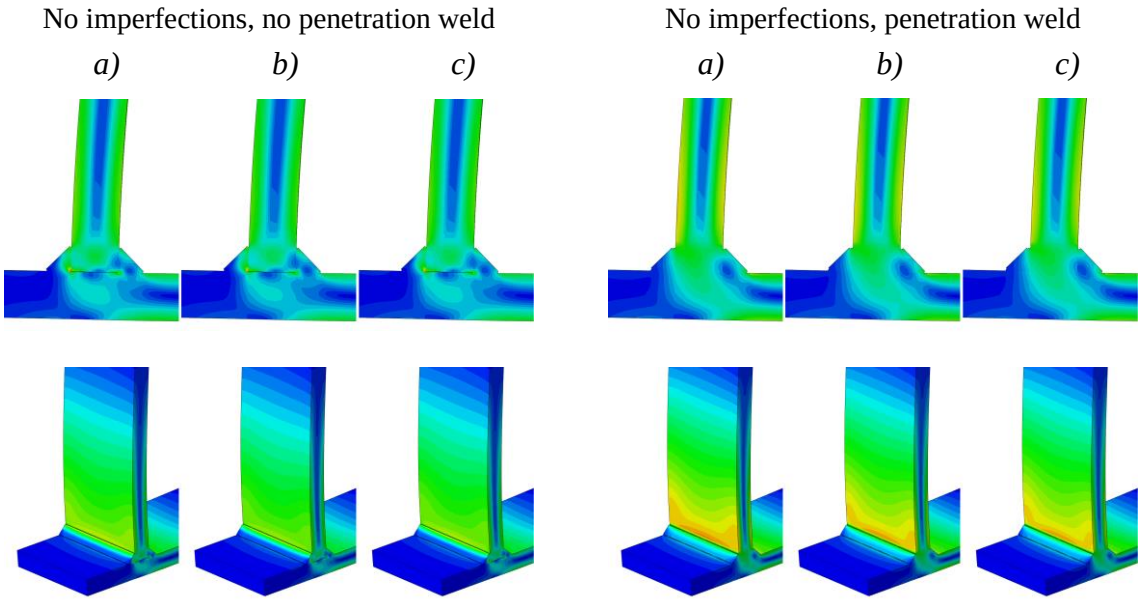

Fig. 14. Results of simulation tests (stresses reduced according to the Huber-Mises-Hencky theory): a) Weld uniform material, b) weld uncooled material, and c) welded helium-cooled material

7. CONCLUSIONS

Structural observations have confirmed that joint structure is affected by thermodynamical conditions (helium or argon m-jet cooling). The structures are completely different. Without micro-jet cooling after welding, expanded ferrite could be observed, which does not guarantee good joint properties. After applying helium m-jet cooling, it is possible to obtain a very favorable fine-grained structure that improves the permanent deformation ability of the joint. Such welds have a favorably low Young's modulus value and a high Poisson's ratio value.

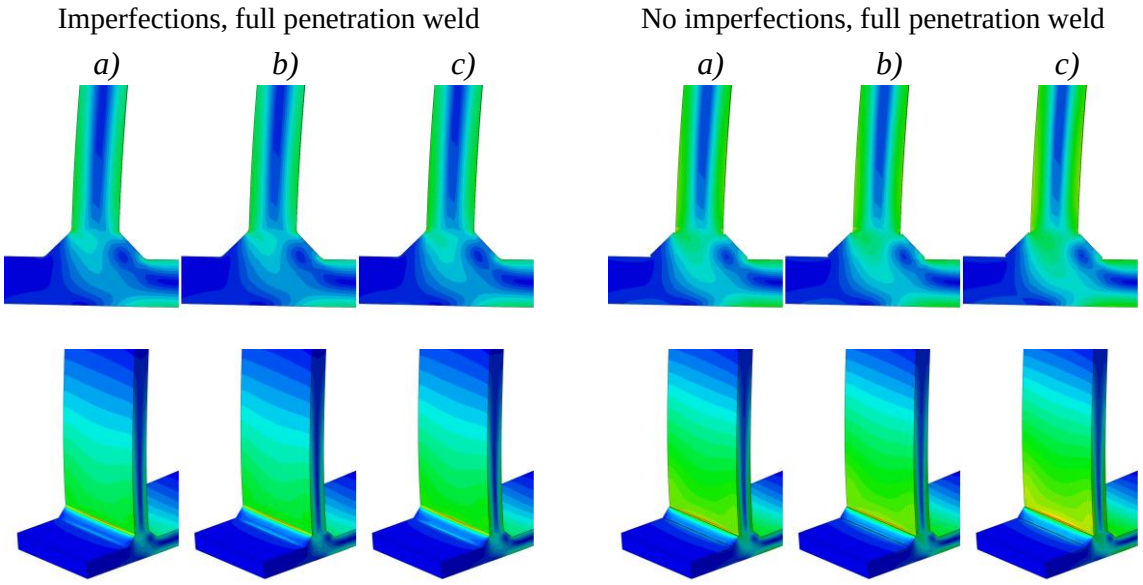

Fig. 15. Results of simulation tests (Stresses reduced according to the Huber-Mises-Hencky theory), a) weld uniform material, b) weld uncooled material, and c) welded helium-cooled material

The article also presents a model that allows the simulation of the collision of a crane trolley with a bumper at the selected speed to calculate the impact force acting on a buffer construction. The presented phenomenological model in connection with the FE model of welded joints and the obtained values of the material parameters of the welded material can provide an abundance of useful information about stress concentration in crane construction. Based on the research carried out, it is important to conduct further analyses, including tests to verify the number of fatigue cycles depending on the weld material cooling process used and the modeling method of the welded joint.

References

1. Izairi, N. & Ajredini, F. & Vevecka-Pfiftaj, A. & Makreski, P. & Ristova, M.M. Microhardness evolution in relation to the Figtalline microstructure of aluminum alloy AA3004. *Archives of Metallurgy Materials*. 2018. Vol. 63(3). P. 1101-1108. DOI: https://doi.org/10.24425/123782.
2. Helrich, C.S. *Analytical Mechanics*. Springer Cham. 2017. P. 51-92.
3. Chatterjee, D. & Patra, A. & Joglekar, H.K. Swing-up and stabilization of a cart-pendulum system under restricted cart track length. *Systems and Control Letters*. 2002. Vol. 47(4). P. 355-364.
4. Haniszewski, T. Modeling the dynamics of cargo lifting process by overhead crane for dynamic overload factor estimation. *J. Vibroeng*. 2017. Vol. 19. No. 1. P. 75-86.
5. Haniszewski, T. & Margielewicz J. & Gąska D. & Opasiak T. New crane bumper design with an energy absorption device system. *Transport Problems*. 2022. Vol. 17. No. 3. P. 6-16. DOI: 10.20858/tp.2022.17.3.01.
6. Autodesk Inventor. *Help Files*. Available at: https://knowledge.autodesk.com.
7. Celin, R. & Burja, J. Effect of cooling rates on the weld heat affected zone coarse grain microstructure. *Metallurgical and Materials Engineering*. 2018. Vol. 24(1). P. 37-44.
8. Darabi, J. & Ekula, K. Development of a integrated micro cooling device. *Microelectronics Journal*. 2003. Vol. 34(11). P. 1067-1074.
9. Hadryś, D. Impact load of welds after micro-jet cooling. *Archives of Metallurgy and Materials*. 2015. Vol. 60(4). P. 2525-2528.
10. Wu, Q. & Wang, X. & Hua, L. & Xia, M. Dynamic analysis and time optimal anti-swing control of double pendulum bridge crane with distributed mass beams. *Mech. Syst. Signal Process*. 2020. Vol. 144. No. 106968. DOI: 10.1016/j.ymssp.2020.106968.

11. Yakubu, G. & Olejnik, P. & Awrejcewicz, J. On the modeling and simulation of variable-length pendulum systems: a review. *Arch. Comput. Methods Eng*. 2022. Vol. 29. P. 2397-2415. DOI: 10.1007/S11831-021-09658-8/FIGURES/42.
12. PN-EN 13001-2:2013. *Bezpieczeństwo dźwignic. Ogólne zasady projektowania. Część 2: Obciążenia*. Warsaw. Polish Committee of Standardization. 57 p. [In Polish: *Security of cranes. General principles for design. Part 2: Loads*].
13. Mathew, N.J. & Rao, K.K. & Sivakumaran, N. Swing up and stabilization control of a rotary inverted pendulum. *IFAC Proceedings Volumes*. 2013. Vol. 10. IFAC.
14. Vaughan, J. & Kim, D. & Singhose, W. Control of tower cranes with double-pendulum payload dynamics. *IEEE Transactions on Control Systems Technology*. 2010.
15. Wu, Q. & Wang, X. & Hua, L. & Xia, M. Improved time optimal anti-swing control system based on low-pass filter for double pendulum crane system with distributed mass beam. *Mech. Syst. Signal Process*. 2021. Vol. 151. No. 107444.
16. Zhao, Y. & Wu, X. & Li, F. & Zhang, Y. Positioning and swing elimination control of the overhead crane system with double-pendulum dynamics. *J. Vib. Eng. Technol*. 2023. Vol. 1. P. 1-8.
17. Lee, J. & Mukherjee, R. & Khalil, H.K. Output feedback stabilization of inverted pendulum on a cart in the presence of uncertainties. *Automatica*. 2015. Vol. 54. P. 146-57.

Received 11.10.2021; accepted in revised form 02.06.2023